Proceedings of ASME 2011 International Design Engineering Technical Conferences & Computers and Information in Engineering Conference
IDETC/CIE 2011
August 29-31, 2011, Washington, DC, USA

DETC2011-48570

CONTROLLED KINETIC MONTE CARLO SIMULATION OF NANOMANUFACTURING PROCESSES

Yan Wang
Woodruff School of Mechanical Engineering
Georgia Institute of Technology
Atlanta, GA 30332

ABSTRACT

Kinetic Monte Carlo (KMC) is regarded as an efficient tool for rare event simulation and has been used to simulate bottom-up self-assembly processes of nanomanufacturing. Yet, it cannot simulate top-down processes. In this paper, a new and generalized KMC mechanism, called controlled KMC or cKMC, is proposed to simulate complete physical and chemical processes. This generalization is enabled by the introduction of controlled events. In contrast to the traditional self-assembly events in KMC, controlled events occur at certain times, locations, or directions, which allows all events to be modeled. The applications of cKMC to several top-down and bottom-up processes are demonstrated.

1. INTRODUCTION

In product and process design, computational tools allow engineers to predict behaviors of products and performance of manufacturing processes. Similar to computer-aided nano-design tools that can be used to design nanoscale products, computer-aided nanomanufacturing (CANM) tools are valuable to design the process of nanomanufacturing. Computing and information technologies will play a significant role in the success of new nanomanufacturing systems. Effectiveness and efficiency must be considered early in the design cycle for maximum impact [1].

In general, nanomanufacturing techniques are classified as either top-down or bottom-up [2,3,4]. In the top-down approaches, materials are removed with low volumes and sizes down to the scale of dozens of nanometers. In the bottom-up approaches, materials are assembled under the guidance of nano-scale templates, either physically or chemically. Simulation is the core methodology of CANM. Molecular dynamics (MD) simulation has been used to study top-down atomic scale machining in the past two decades [5]. MD was used to simulate nano-lithography [6,7] and cutting with diamond tools [8,9,10,11]. For other processes, MD has been used to simulate nano-indentation [12], laser ablation of bulk materials [13], and laser-based sintering [14]. However, the major issue of MD is its short time scale that is not compatible with those in nanomanufacturing. MD simulates behaviors at the time scales ranging from femto to nano seconds. Most of the computational time in MD is spent on the thermal vibration of atoms, instead of our interested processes that are usually longer than microseconds. Those events of interest with longer time scale than thermal vibration are rare events. MD simulation is very inefficient in simulating these rare events. Unrealistic assumptions have to be made to accommodate the time scale. For instance, extremely high cutting speed (e.g. 100 m/second) was used in the above MD simulation studies, which only simulate pico seconds of the processes. The accuracy of predictions on required forces, defects, and others is affected.

To simulate the rare events of transitions or reactions, several improvements of MD have been proposed to bridge the gap of time scale and accelerate the simulation speed of rare events, such as by running multiple trajectories [15], introducing bias potentials [16], or increasing temperatures [17]. However, the inherent inefficiency of MD is that computational time is spent on trajectory prediction, which is not important for rare event simulations. Compared to MD, atomic scale kinetic Monte Carlo (KMC) [18,19] is more efficient in simulating the infrequent transition processes with times longer than thermal vibrations.

In KMC, various discrete *events* or *processes* are defined. During simulation, the discrete events are generated and fired sequentially based on their respective probabilities of occurrence, which are usually assumed to be exponential distributions. These probabilities can be calculated from the reaction or transition rate constants, which could be estimated from either experiments or first-principles calculations.

KMC has been widely used to simulate chemical reactions and some of the bottom-up self-assembly processes such as chemical vapor deposition and physical vapor deposition. Yet, it has not been considered to simulate general

nanomanufacturing processes, particularly those top-down processes. In this paper, a novel and generic KMC simulation mechanism is proposed to simulate nanomanufacturing processes. The new mechanism is called controlled kinetic Monte Carlo (cKMC). The goal is to provide an efficient and unified simulation framework for CANM to enable both top-down and bottom-up nanomanufacturing processes.

For the rest of the paper, the background overviews of nanomanufacturing and KMC are first given in Section 2. In Section 3, the cKMC simulation framework is proposed and illustrated by several top-down and bottom-up processes. The implementation details are described in Section 4.

2. BACKGROUND

This section first gives an introductory overview of various nano-fabrication techniques that are relatively well developed and promising for commercialization in the near future. Then KMC and its applications in self-assembly processes are summarized.

2.1 Nanomanufacturing

Many of the nanomanufacturing techniques are inherited and extended from the traditional semiconductor manufacturing techniques, since semiconductor is one of the major driving forces for nanomanufacturing.

2.1.1 Top-Down Approaches

Most top-down nano-fabrications are for surface patterning. By patterning local surface regions of a solid substrate with nanoscale features, the substrate has the ability to recognize specific nanostructures. Some patterning methods are developed to write nanoscale features, others are to replicate. The well developed patterning methods include scanning probe lithography, focused beam lithography, soft lithography, and nanoimprint lithography.

The scanning probe lithography techniques [20] are mechanical approaches to realize patterning. Typically small (<50nm) tips or probes are used to scan near the surface of a sample. Originally designed for imaging purposes, they can also be used to perform sophisticated lithography. The tips can be used to alter the structure of materials. Different configurations have been developed, such as scanning tunneling microscopy [21], atomic force microscopy (AFM) [22], and scanning electrochemical microscopy [23].

Focused beam lithography is the process of scanning a beam of electrons or ions across the resist surface and generate patterns by selectively exposing and removing the resist. This can be done on a modified electron microscope. In electron beam lithography, a high-energy electron beam can be used to form patterned nanostructures [24] or material deposition [25,26]. Focused ion beam (FIB) lithography [27] is another high-resolution patterning method where ion beam is used. It has been used in semiconductor industry mainly for mask repairing, device modification and analysis and is also good for precise ion milling tool [28,29], gas-assisted etching [30,31], and induced material deposition [32].

Soft lithographies [33,34] are techniques to fabricate or replicate structures by stamps, molds, and conformable photomasks made from elastomeric materials, most notably polydimethylsiloxane (PDMS). High-resolution elastomeric stamp are used to print with chemical inks capable of forming a self-assembled monolayer on a target substrate. Recently PDMS elements were used as optical components for patterning structures in photosensitive polymer [35].

Nanoimprint lithography (NIL) [36,37] is able to replicate sub-10 nm patterns with high throughput. It uses a hard mold (e.g. Si, SiO_2, and SiC) that contains nanoscale features to emboss into polymer materials and cast on the substrate under controlled temperature and pressure conditions, which can be further transferred through the resist layer via etching processes. Recent research focuses on seeking new materials, e.g. metallic glasses [38], to improve the durability of molds.

2.1.2 Bottom-Up Approaches

In bottom-up approaches, nanoscale structures are synthesized by self-assembly with physical or chemical guidance. Self-assembly is a parallel process in nature. However, it is more difficult to achieve controllable atomic-level precision compared to the top-down approaches.

Chemical vapor deposition (CVD) [39] is a relatively matured coating process which involves the dissociation and chemical reactions of gaseous reactants in an activated (heat, light, plasma) environment, followed by the formation of a stable solid product. It has been widely used in ceramic and semiconductor industry. A CVD process involves chemical reactions in the gas phase, and chemisorption and desorption on the substrate surface. For nanoscale structures, CVD has been used to grow arrays of carbon nanotubes [40,41] and ZnO nanowires [42] on substrates. Several variants of CVD have been developed, such as electrostatic spray assisted vapor deposition, combustion chemical vapor deposition, metal organic chemical vapor deposition, and aerosol assisted chemical vapor deposition, to use more environmentally friendly precursors and facilitate chemical reactions. Recently, it was demonstrated that complex 3D nanostructures can be fabricated by CVD induced by focused ion beams [43].

Physical vapor deposition (PVD) [44,45] is a variety of surface coating methods in which target materials are evaporated by electron beam, ion beam, plasma, or laser. The evaporant material is vaporized with the supplied energy and solidified on the surface of substrate. Different from CVD, there are no chemical reactions involved in PVD. PVD processes usually require a high vacuum environment, both to allow the vapor to reach the substrate without reacting with other gas-phase atoms in the chamber, and to reduce the impurity of deposited films. Most used PVD processes include magnetron sputtering, molecular beam epitaxy, arc vapor deposition, ionized PVD, etc.

Dip-pen nanolithography (DPN) is a scanning probe microscopy-based nano-fabrication technique that uniquely combines direct-write soft-matter compatibility with the high resolution and registry of AFM [46,47]. It uses an ink-coated AFM tip to pattern a surface. Unlike the scanning probe

lithography methods, DPN is a direct-write constructive lithography that allows for printing from scanning probe tips onto a surface with sub-50-nm resolution, and no premodification of the surface through energy delivery (such as ultraviolet and ion- or electron-beam irradiation) is required prior to the material delivery process. To increase fabrication throughput, parallel DPN tips were demonstrated [48]. Rather than cantilevers, polymer pen lithography [49] uses a soft elastomeric tip array.

2.2 Kinetic Monte Carlo Simulation and Its Applications

KMC is a useful tool to simulate systems at multiple time scales with rare events. In this section, the introductions of KMC and its application in some bottom-up self-assembly processes are given.

2.2.1 Kinetic Monte Carlo Simulation

In KMC, various discrete events (also called *processes*) are defined. For instance, in the CVD process of crystal growth, the major types of events include: *adsorption* (particles in vapor are attracted to the solid surface), *desorption* (particles previously absorbed on the solid surface escape and are vaporized), *diffusion* (particles on the surface or in the solid move to a different location), and *surface reaction* (gas precursors react and generate solid products).

During KMC simulation, discrete events are generated and fired sequentially based on their respective probabilities of occurrence, which are exponential distributions in general. The transition rate (also called propensity function) k_j from current state to state j is proportional to $\exp(\Delta E_j/k_BT)$, i.e. $k_j = \nu_j \exp\left(-\Delta E_j / k_B T\right)$, where k_B is the Boltzmann constant, T is the temperature, ΔE_j is the energy barrier between the current state and state j, and ν_j is the pre-exponential factor that can be measured or calculated from the vibrational frequencies, e.g. based on the harmonic transition state theory [50,51].

Among all M possible transition paths leaving current state, the transition probability p_j to state j is $p_j = k_j / \sum_{i=1}^{M} k_i$. Because the time between transition events X_j is exponentially distributed as $X_j \sim \exp(k_j)$, and the probability that the inter-arrival time of event j is the minimum among M independent events is $\Pr[X_j = \min(X_1,\ldots,X_M)] = k_j / (k_1 + \cdots + k_M)$. Once event j is fired with the probability p_j, the time of the system is advanced by another random value $t \sim \exp\left(k_1 + \cdots + k_M\right)$, which is the earliest occurring time for any one out of the M independent events that are exponentially distributed. This event selection and clock advancement algorithm is the most used one and often referred as the direct method [52]. Other algorithms are also available [18,19].

KMC is an effective solution for rare event simulation. Yet it faces three major technical challenges. First, ideally all events have to be known a priori and listed in the event catalog so that the dynamics of physical process can be simulated accurately. Second, during simulation the occurring probabilities of events are assumed to be accurate and fixed. Third, the time scales of the events may vary significantly, thus computational time is not optimized to focus more on slower but critical events. Recently, some solutions were proposed to resolve some of the above issues. The current paper will not address these issues. See [53] for more information.

2.2.2 KMC Simulation of Self-Assembly Processes

In the domain of nanomanufacturing, KMC simulation has been used in some of the bottom-up processes. For PVD, it is used to simulate deposition and diffusion events in sputtering (e.g. [54,55]). The additional research question is how to incorporate extra information of kinetic energy in particles to make correct predictions, such as reflection, resputtering, latent heat, kinetic energy induced diffusion, and others [56,57,58]. Approximations based on molecular dynamics and the embedded atom method are applied. For CVD processes, KMC is used to simulate on-site chemical reaction events of film growth (e.g. [59,60,61,62]) and etching (e.g. [63,64,65]).

The major issue in KMC simulation of bottom-up self-assembly processes is the accuracy of reaction or transition rates used in simulation, because not much experimental data are available. Alternatively, the rates can be estimated by first-principles simulation. Efforts to integrate density functional theory and KMC have been taken to simulate CVD processes of diamond growth [66], molecular beam epitaxial growth of compound semiconductors [67], catalytic decomposition and surface reaction [68], and others.

KMC simulation has not been applied in top-down processes. The main reason is that the traditional KMC has no direct control on where and when an event takes place. They are stochastically determined by random sampling. In top-down processes, stochastic events are mixed with deterministic ones, where precise locations of manipulation are controllable. In this paper, a generalized KMC mechanism, called controlled KMC, is proposed to simulate both bottom-up and top-down processes.

3. THE PROPOSED CONTROLLED KINETIC MONTE CARLO SIMULATION

In the bottom-up processes, the simulated events mainly include thermally or chemically induced atomic rearrangements such as diffusion, absorption, desorption, surface reaction and abstraction. These rearrangements occur spontaneously in the form of self-assembly. Those spontaneous events are called *self-assembly events*. In the top-down processes, the atomic rearrangement is triggered by some external energy sources such as force or light. The rearrangement is further induced by self-assembly events. These external events could be scanning probe tip interaction with samples, bombardment of high-energy particles, molding materials with attractive and repulsive forces, and others. These external events are scheduled to occur at certain locations or at particular times to control the overall process. Therefore, they are called *controlled events*. The major new concept in cKMC is the

introduction of controlled events in the algorithm in order to simulate top-down processes in parallel with bottom-up processes.

Similar to the traditional KMC, if M available self-assembly events with the rates of $k_j(t)$'s ($j = 1,\ldots,M$) at a particular time t in the system, the probability that event j is chosen to be the next event is $p_j = k_j(t) / K(t)$ where $K(t) = \sum_{j'=1}^{M} k_{j'}(t)$. Notice that the propensity functions k_j's (thus the total propensity K) and the number of available events M are time-dependent. After one event is fired, the clock advances by $\Delta t = -\ln(u) / K$ where $u \sim U(0,1)$ is a random number uniformly distributed between 0 and 1.

The main parameters for both self-assembly and controlled events are how often the events occur, specified as rates. Additional parameters are introduced for controlled events, including when and where the events may occur. When controlled events occur could be deterministic. For example, in the AFM nanolithography, the time when the cutting tip reaches one particular position along the predetermined path is fixed. Furthermore, the spatial location where a controlled event occurs could also be predetermined. For example, in kinetic energy induced diffusion (e.g. ions or electrons in focused beam lithography under electromagnetic field), the preferred directions that particles move towards are fixed. Therefore in the cKMC simulation, there is a time, a direction vector, or both associated with a controlled event. As the simulation clock is advanced based on self-assembly events, controlled events are checked constantly so that those with the predetermined time earlier than the current time should be fired. If a predetermined direction is associated with a controlled event and the reaction or transition direction is different, then the event is aborted. More details will be described in the following sections.

Notice that the particles in the KMC are not necessarily atoms only. They could be electrons, photons, monomers, or molecules, as long as the inside structure and behavior are not of interest and assumed to be at an equilibrium state. It also should be noted that controlled events are not only necessary to simulate top-down processes, but also useful for some bottom-up processes such as controlled growth of carbon nanotube with directed orientations, which so far still largely depends on MD simulation.

3.1 Scanning Probe Lithography

For the scanning probe lithography process in Fig. 1, besides the regular *workpiece species*, there is a *controlled species*, even though chemically they could be identical. Controlled species are species where the times of associated events are deterministic. That is, the events will be fired at pre-scheduled times. In this case, it is based on the moving speed of the probe. The locations of controlled species are also pre-determined based on the planned scanning or cutting path. There is also a *vaporized workpiece species* which escapes the solid body of workpiece in regular diffusion. In the controlled reaction of the controlled species, atoms of the controlled species are converted to *activated control species* based on the scheduled times sequentially. Here, the probe is moving along the path denoted by the sites of controlled species along the x-axis direction from left to right. The atoms of controlled species on the left have earlier time of conversion than those on the right. The activated control species has a higher kinetic energy than the vaporized workpiece species. Therefore, they are associated with *controlled diffusion events*. The controlled diffusion events have several restrictions, such as the *controlled directions* (illustrated by the dotted arrows in Fig. 1) by which activated atoms can diffuse to neighboring sites or by which they can interact with neighboring atoms of workpiece species. In addition, vacancy exists between occupied spatial lattices. Therefore, a *vacancy species* can be defined. Finally, there is an *absorbent species* at the boundary of simulated domain, where the lifecycle of the atoms of vaporized workpiece species and controlled species are terminated.

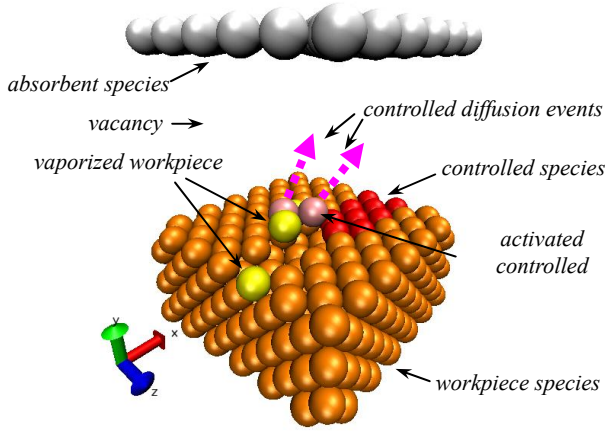

Fig. 1: Illustration of scanning probe lithography events

In the simplified scanning probe lithography process in Fig. 1, several example events are listed in Table 1. Events are organized into several categories based on the number of neighboring sites involved. Events are denoted by reaction alike equations. The left of equations are reactants and the right are products. The first reactant is the owner of the event, meaning that the event is associated with the site where the first reactant initially resides. After the reaction, the reactant species are replaced by the product species at the corresponding sites. Among the events in Table 1, reaction R1 has only one site involved. It is a controlled event when the controlled species is converted to the activated controlled species based on the scheduled time along the cutting path. R2 to R6 have two neighboring sites involved. R2 is the controlled diffusion event associated with activated controlled species. It models the effect of kinetic energy associated with particles transferred from the moving probe. A particle of activated controlled species can diffuse to a vacant neighboring site if the direction from the current site to the vacant site is aligned with the controlled direction. In contrast, R3 and R4 are regular

diffusion events without directional constraints. R5 and R6 absorb particles at the boundary of simulation. Among the reactions with three reactants, R7 is a coordinated diffusion event where three sites are involved. It has been revealed by first-principles simulation that coordinated diffusion with multiple sites involved could have lower energy barriers than the traditional single-hop diffusion (e.g. in R4) as originally thought [69,70]. R8 is an adsorption event. For reactions with four reactants, R9 is an example interaction between the activated controlled species and the workpiece species where kinetic energy is transferred. R10 is another absorption event where kinetic energy of activated controlled species is absorbed and atoms settle down. It should be noted that Table 1 only lists some examples. More events can be introduced in a similar format, which allows for necessary refinement and extension.

Table 1: Example events in scanning probe lithography

Number of sites involved	Reaction/transition event
1	R1: *controlled_species* → *activated_controlled_species* (controlled)
2	R2: *activated_controlled_species* + *vacancy* → *vacancy* + *activated_controlled_species* (controlled) R3: *vaporized_workpiece_species* + *vacancy* → *vacancy* + *vaporized_workpiece_species* R4: *workpiece_species* + *vacancy* → *vacancy* + *workpiece_species* R5: *vaporized_workpiece_species* + *absorbent* → *vacancy* + *absorbent* R6: *activated_controlled_species* + *absorbent* → *vacancy* + *absorbent*
3	R7: *workpiece_species* + *workpiece_species* + *vacancy* → *vacancy* + *workpiece_species* + *workpiece_species* R8: *vaporized_workpiece_species* + *workpiece_species* + *workpiece_species* → *workpiece_species* + *workpiece_species* + *workpiece_species*
4	R9: *activated_ controlled_species* + *workpiece_species* + *vacancy* + *vacancy* → *vacancy* + *workpiece_species* + *vacancy* + *vaporized_workpiece_species* R10: *activated_ controlled_species* + *workpiece_species* + *workpiece_species* + *workpiece_species* → *workpiece_species* + *workpiece_species* + *workpiece_species* + *workpiece_species*

The controlled events can be generally used in various complex top-down fabrication processes. In MD simulation, special treatments of potential energy between atoms of workpiece and tool are needed so that the rapid movement of atoms can be modeled. Here, controlled events are used to model the special movement of atoms under directional constraints.

3.2 Focused Beam Lithography

In focused beam lithography, high-energy particles such as ions or electrons are projected to workpieces to modify structures locally via physical or chemical interactions. The obvious advantage of KMC approaches is that chemical reactions can be simulated easily. The proposed cKMC can simultaneously simulate the controlled physical interactions and chemical reactions. Therefore, more complex processes such as FIB assisted chemical vapor deposition can be simulated in the same way.

As illustrated in Fig. 2, the controlled species is the source of ions (e.g. gallium and gold/silicon alloy) or electron beams. They are selectively allocated to some lattice locations based on the specified milling path. When the controlled species is activated based on its predetermined schedule, it becomes the ion or electron that diffuses in the specified direction. When ions or electrons hit workpiece species, kinetic energy is transferred and gas molecules of workpiece species are generated. Chemical reaction and electron transfer can also be involved. For instance, the secondary ions of workpiece species and electrons can be generated.

Table 2 lists some examples of FIB lithography processes, assuming gallium ion is applied. R1 is the controlled event where gallium ions Ga^+ are generated according to the predetermined schedule. The locations of the controlled species *Ga_src* are also predetermined based on the milling path. R2 is the controlled trajectory of ions. R3-R6 are desorption paths of vaporized workpiece species, secondary ions of workpiece species, neutralized gallium, and electrons respectively. If the directions of paths are known, they can be controlled events too. R7-R10 define the simulation boundary. R11-R12 are examples of interaction between gallium ions and workpiece.

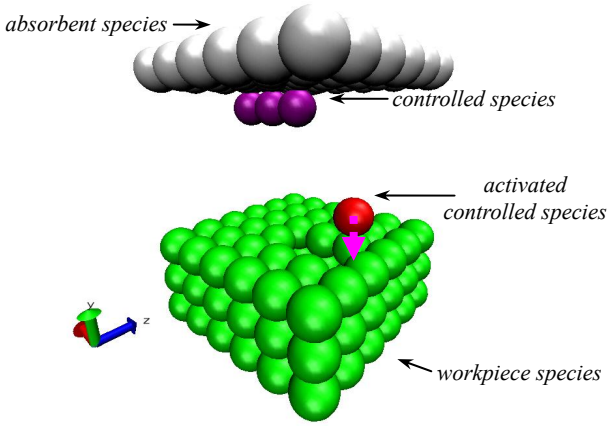

Fig. 2: Illustration of focused beam lithography events

Table 2: Example events in FIB lithography processes

Number of sites involved	Reaction/transition event
1	R1: *Ga_src* → Ga^+ (controlled)
2	R2: Ga^+ + *vacancy* → *vacancy* + Ga^+ (controlled) R3: *workpiece_species_gas* + *vacancy* → *vacancy* + *workpiece_species_gas* R4: *workpiece_species*$^+$ + *vacancy* → *vacancy* + *workpiece_species*$^+$ R5: *Ga_gas* + *vacancy* → *vacancy* + *Ga_gas* R6: e^- + *vacancy* → *vacancy* + e^- R7: *workpiece_species_gas* + *absorbent* → *vacancy* + *absorbent* R8: *Ga_gas* + *absorbent* → *vacancy* + *absorbent* R9: *workpiece_species*$^+$ + *absorbent* → *vacancy* + *absorbent* R10: e^- + *absorbent* → *vacancy* + *absorbent*
3	R11: Ga^+ + *workpiece_species* + *vacancy* → *Ga_gas* + *vacancy* + *workpiece_species_gas* R12: Ga^+ + *workpiece_species* + *vacancy* → *Ga_gas* + e^- + *workpiece_species*$^+$

3.3 Nanoimprint Lithography

Nanoimprint lithography is a promising approach to achieve high-precision high-throughput nanoscale patterning. Fig. 3 illustrates the cKMC simulation of nanoimprint lithography. The mold may be represented by several controlled species at different locations. In the example shown in Fig. 3, the mold moves in the *y* direction. Equivalently in the implemented model, the controlled species are converted to vacancies gradually from bottom to top based on the specified speed. The interaction between the mold and the resist mobilizes the resist particles, which results in the situation that the geometry of pattern is not perfectly printed.

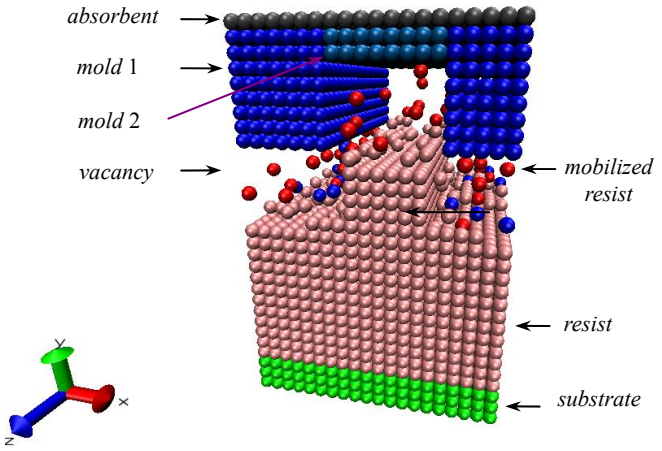

Fig. 3: Illustration of nanoimprint lithography events

Table 3 shows some example events in the nanoimprint lithography process. R1 and R2 are controlled events where the controlled species are converted to vacancies in a controlled and deterministic manner. R3 characterizes the diffusion of mobilized resist species. R4 defines the boundary of simulated domains. R5 and R6 capture the interaction between the mold and the resist, where resist species may be mobilized. R7 is the adsorption process where mobilized resist species settle down.

Table 3: Example events in nanoimprint lithography processes

Number of sites involved	Reaction/transition event
1	R1: *mold*1 → *vacancy* (controlled) R2: *mold*2 → *vacancy* (controlled)
2	R3: *mobilized_resist* + *vacancy* → *vacancy* + *mobilized_resist* R4: *mobilized_resist* + *absorbent* → *vacancy* + *absorbent*
3	R5: *mold*1 +*vacancy* + *resist* → *mold*1 + *mobilized_resist* + *vacancy* R6: *mold*2 +*vacancy* + *resist* → *mold*2 + *mobilized_resist* + *vacancy* R7: *mobilized_resist* + *resist* + *resist* → *resist* + *resist* + *resist*

In summary, it has been shown in this section how the proposed cKMC mechanism can be used to simulate top-down processes. Scanning probe lithography, focused beam lithography, and nanoimprint lithography are used to illustrate the mechanism. For soft lithography, it is similar to the nanoimprint lithography, except that the detailed events and reaction rates need to be fine-tuned to reflect the specific processes. For photosynthesis type of processes, it is similar to the focused beam lithography where photons replace ions. Local self-assembly and chemical reactions can be easily incorporated as either self-assembly or controlled events.

Bottom-up processes can also be simulated by the cKMC simulation. In traditional KMC, bottom-up processes are simulated based on self-assembly events. Controlled events are useful in simulating some of the bottom-up processes, where traditional KMC is not capable of. For instance, in UV ablation of Polymethylmethacrylate (PMMA) [71], radical photochemical reactions cause bond-breaks with new species generated, explosion of volumes, and particles ejected. In these cases, controlled events are reactions at selected locations. At a lower UV energy level, photothermal effects will cause melting and evaporation. Controlled events in this case are thermal diffusions. In ionized PVD, plasma particles only move within a confined space subject to electromagnetic fields to ionize vaporized metals. Ionized inert gas molecules such as argon travel and hit target metals under the guidance of electrical fields. These are also controlled events. In the following Section 3.4, ionized PVD is used to show how cKMC can simulate complete bottom-up processes.

3.4 Ionized Physical Vapor Deposition

Ionized PVD is an extension of the PVD technology that can achieve directional deposition of metals on substrates with high-aspect ratio features, such as vias and trenches. In the traditional PVD, it is difficult to let metal vapor travel deep enough into the bottom of vias. In ionized PVD, the sputtered or evaporated metal atoms go through the plasma sheath above substrate and ionized. External electrical field then guide ionized metal gas that can travel towards the bottom of vias.

The cKMC simulation of ionized PVD is shown in Fig. 4. There are an electron source and an argon gas source which inject electrons and argon gas into the domain. The plasma is generated and confined between the target and the substrate. Some examples of events are listed in Table 4. R1 and R2 are injection of argon gas and electrons. R3 to R5 are diffusions of argon (Ar), argon at the excited state (Ar^*), and ionized argon (Ar^+) respectively. Ar^* is generated by collision between electron and argon as in R10, and Ar^+ is generated by collision between electron and Ar^* as in R11. Similarly, R6 to R8 are diffusions of metal (M), metal at the excited state (M^*), and ionized metal (M^+) respectively. M^* is generated by collision between electron and metal as in R12, and M^+ is generated by collision between electron and M^* as in R13. Particularly, the diffusions of ionized argon (R5) and ionized metal (R8) are controlled events where the directions are controllable. R10 to R13 are also controlled where the collisions with electrons are towards the confined space of plasma sheath. R14 and R15 are adsorption events. Among events where three sites are involved, R16 and R17 are one-step ionization, where ionized argon and metal are generated from argon and metal directly without intermediate excited states. R18 is the metal ionization

by collision with argon at the excited state. R19 is the bombardment of the target by ionized argon gas and metal atoms are sputtered out of the target. R20 to R23 are also adsorption events.

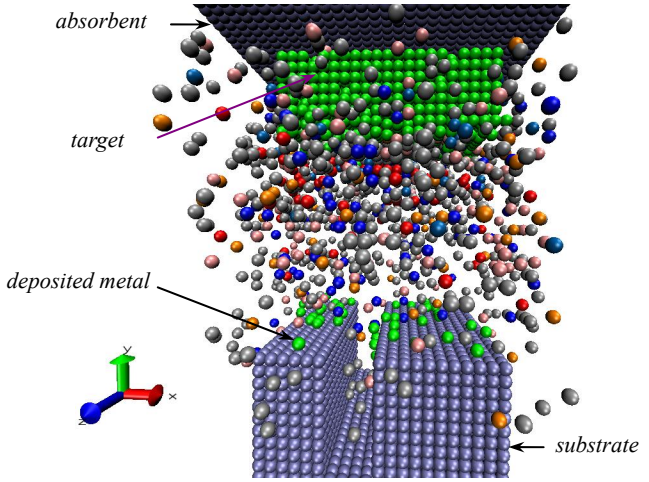

Fig. 4: Illustration of ionized physical vapor deposition events

Table 4: Example events in ionized PVD processes

Number of sites involved	Reaction/transition event
2	R1: $Ar\_src + vacancy \rightarrow Ar\_src + Ar$ R2: $e\_src + vacancy \rightarrow e\_src + e^-$ R3: $Ar + vacancy \rightarrow vacancy + Ar$ R4: $Ar^* + vacancy \rightarrow vacancy + Ar^*$ R5: $Ar^+ + vacancy \rightarrow vacancy + Ar^+$ (controlled) R6: $M + vacancy \rightarrow vacancy + M$ R7: $M^* + vacancy \rightarrow vacancy + M^*$ R8: $M^+ + vacancy \rightarrow vacancy + M^+$ (controlled) R9: $e^- + vacancy \rightarrow vacancy + e^-$ R10: $e^- + Ar \rightarrow Ar^* + e^-$ (controlled) R11: $e^- + Ar^* \rightarrow Ar^+ + e^-$ (controlled) R12: $e^- + M \rightarrow M^* + e^-$ (controlled) R13: $e^- + M^* \rightarrow M^+ + e^-$ (controlled) R14: $M + substrate \rightarrow target + substrate$ R15: $M + target \rightarrow target + target$
3	R16: $e^- + Ar + vacancy \rightarrow Ar^+ + e^- + e^-$ R17: $e^- + M + vacancy \rightarrow M^+ + e^- + e^-$ R18: $Ar^* + M + vacancy \rightarrow M^+ + Ar + e^-$ R19: $Ar^+ + target + vacancy \rightarrow e^- + Ar + M$ R20: $M + substrate + substrate \rightarrow target + substrate + substrate$ R21: $M^+ + substrate + substrate \rightarrow target + substrate + substrate$ R22: $M^+ + substrate + target \rightarrow target + substrate + target$ R23: $M^+ + target + target \rightarrow target + target + target$

4. IMPLEMENTATION AND DEMONSTRATION

4.1 Implementation

The proposed cKMC is implemented in C++ and integrated with SPPARKS [72], which is an open-source KMC toolbox developed at the Sandia National Laboratories. The key components of the cKMC are the controlled species and controlled events.

Controlled species are specified by the input script "***control_species*** *reactant rate product x y z neighbor_lower neighbor_upper init_time*" where ***control_species*** is the command, *reactant* is the name of controlled species, *product* is the resultant species in the controlled reaction, *rate* is the numerical value of reaction rate, and *x*, *y* and *z* specify the direction along which the reaction occur. That is, the reactants of controlled species react and convert to products sequentially along the specified direction at the rate. The next two integer values, *neighbor_lower* and *neighbor_upper* specify the lower and upper bounds of neighboring sites where the controlled species may react. If the number of its neighbors is not within the bound, the controlled reaction is not initiated. This provides more controls on where controlled reactions can occur. Finally *init_time* specifies when the controlled reaction is started.

Events are specified by the input script "***event*** *reactant*_1 (*reactant*_2, etc.) *rate product*_1 (*product*_2, etc.)" where ***event*** is the command, *rate* is the numerical value of reaction rate, and corresponding reactants and products at the particular site are defined. For instance, after the event is fired, reactant_1 is replaced by product_1, reactant_2 by product_2, and so on.

Controlled events are specified in two types. The first type is by the direction along which the reaction is going towards, and the second one is by the target location where the reaction is targeted at. The input script is "***control_event*** *index dx dy dz x*0 *y*0 *z*0 *theta neighbor_lower neighbor_upper*" where ***control_event*** is the command, *index* refers to the event index previously specified by the command ***event***, *dx*, *dy* and *dz* specify the direction which the first and second reactants should aligned with, and *theta* is an angular allowance such that the direction formed by the first and second reactants can be within the range of +/− theta and the reaction still occurs. In other words, the controlled events provide directional selections of events. Controlled events are only fired if the direction formed by the first two reactants is the specified direction or close enough within the +/− theta range. Before a controlled event is inserted into the event list, the directional criterion is checked. Those controlled events that do not satisfy the constraints are disregarded. When *dx*=*dy*=*dz*=0, *x*0, *y*0 and *z*0 take effect and they specify the target location by which the direction of reaction is from the current site to the target location. Two cases can be specified. When *theta* is positive, the reaction direction "converges" towards the target location. When *theta* is negative, the reaction direction "diverges" away from the target location. Similarly, if the direction formed by the first two reactants is far from the specified, events are discarded. Again, *neighbor_lower* and *neighbor_upper* specify the lower and upper bounds of neighboring sites where the controlled event may occur. Therefore, rather than directly modeling kinetic energy, controlled events provide a directional selection for cKMC.

Before a simulation starts, all species, sites, and events are specified by script commands. Internally species, controlled species, events, controlled events, reaction sites and others are stored in array-type data structures. For each site where a controlled species resides, there is an associated *keyvalue*,

which usually is the time when the controlled reaction occurs at site j of controlled species i, which is calculated as $t_{ij} = t_i^0 + \left(\mathbf{r}_{ij} \cdot \mathbf{s}_i - d_i\right) / a_i$ where t_i^0 is the reaction start time for controlled species *i* as previously specified by *init_time*, $\mathbf{r}_{ij}$ is the 3D coordinate of site *j* of i^{th} controlled species, $\mathbf{s}_i$ is the direction of controlled reaction for controlled species *i*, d_i is calculated as $d_i = \min_j \left(\mathbf{r}_{ij} \cdot \mathbf{s}_i\right)$, and a_i is the reaction rate for controlled species *i*. In this way, the sites of controlled species are sorted based on the keyvalues corresponding to the reaction direction so that the controlled reactions can be fired deterministically and the time is controllable. Nevertheless, keyvalues can be values other than times if necessary.

Table 5 lists the pseudo-code of the implemented cKMC algorithm.

Table 5: The implemented cKMC algorithm

```
Initiate regular lattice sites;
Specify regular species on each regular site;
FOR i = 1 : numControlSpecies
      generate the list controlSpeciesSites_i for the i^th controlled species;
      calculate keyvalue of the i^th controlled species;
      sort controlSpeciesSites_i based on keyvalue;
END
Define all possible events;
Specify controlled events;
WHILE stop criteria are not met
      Update a list of J active sites with sitePropensity_j > 0 for site j
         where sitePropensity_j = sum_k propensity_jk is sum of all event propensities
         at site j
      Update totalProp = sum_{j=1}^{J} sitePropensity_j;
      //choose a site for the next event
      Generate r_1 ~ Uniform(0,1);
      Find m^th site where sum_{j=1}^{m-1} sitePropensity_j < totalProp * r_1 <= sum_{j=1}^{m} sitePropensity_j;
      //choose an event from the chosen site
      Generate r_2 ~ Uniform(0,1);
      Find n^th event where sum_{k=1}^{n-1} propensity_mk < sitePropensity_m * r_2 <= sum_{k=1}^{n} propensity_mk;
      Fire event n at site m and update species at neighboring sites;
      //update event list
      FOR all events associated with site m that are not controlled
          OR events are controlled AND controlled event criteria are met
             Add the event into the event list of site m;
      END
      Update propensities for site m and neighboring sites;
      //update system time
      Generate r_3 ~ Uniform(0,1);
      Advance system time T to T + Δt where Δt = -ln r_3 / totalProp;
      //update the status of controlled species sites
      FOR i = 1 : numControlSpecies
            Fire all controlled events in controlSpeciesSites_i with keyvalue < T;
      END
END
```

4.2 Demonstration

To demonstrate the effectiveness of the cKMC simulation, an example of NIL is used. Fig. 5-(a) shows a scanning electron microscopy (SEM) image of a PMMA layer imprinted by a Chromium (Cr) stamp with an array of columns [73]. The columns have diameters of 50 nm and heights of 60 nm. The array of columns has a 100nm period. Fig. 5-(b) shows the constructed cKMC model, which consists of 93,312 simple cubic sites. Each site has 26 neighbors. The area of the PMMA resist is 100nm by 100nm, which is modeled as 38 by 38 sites. Given that the covalence radius of Cr is about 0.139 nm and the distance between atoms is 0.278 nm, each particle in the cKMC model represents about 10×10×10 atoms.

Compared to other top-down processes, this example of nanoimprint lithography is more complex and interesting. Large deformation of PMMA resist is observed. Therefore, this example is chosen to demonstrate the sophistication that cKMC can achieve. When the deformation of resist is not significant as in scanning probe lithography and focus beam lithography, some of the controlled events for kinetic energy and mass transfer can be omitted in simulation and the model can be further simplified.

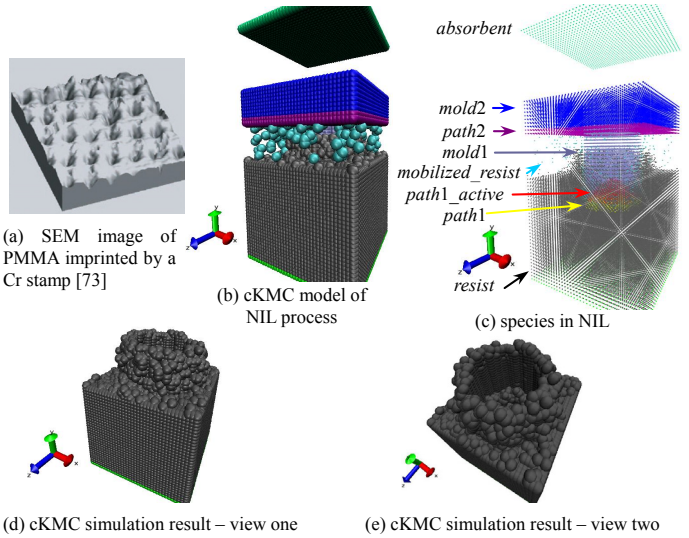

(a) SEM image of PMMA imprinted by a Cr stamp [73]

(b) cKMC model of NIL process

(c) species in NIL

(d) cKMC simulation result – view one

(e) cKMC simulation result – view two

Fig. 5: cKMC model of NIL and the comparison between simulation and the SEM image from an experiment of a PMMA layer imprinted by a Cr stamp

The species and events used in the simulation are listed in Table 6. Fig. 5-(c) shows the different species in simulation. Before the simulation starts, controlled species *path*1 defines the top-down traveling paths for the arrays of columns whereas controlled species *path*2 defines the paths for the top portion of the mold. As simulation starts, *path*1 converts to *path*1_*active* at a preset speed specified by R1, similarly for *path*2 specified by R2, as the mold moves down. R3 and R4 model the upward movement of mold after it reaches the target position in press. Events of R3 and R4 start when the simulation clock reaches a pre-set time. Species *path*1_*active* is used to model the kinetic energy transfer between columns and resist while the mold is being pressed down, as shown R5. As the mold moves down, the column of mold presses resist towards sides. R8 and R11 model the resist particles being dislocated to vacant space, and at the same time *path*1_*active* is converted to *mold*1 that will be used in the upward movement of the mold later. These events mainly occur at the boundary of column where *vacancy* is available. For the inner portion of the column, the controlled event R5 models kinetic energy and mass transport. The direction of the event diverges away from the center of the column in its bottom. Here *path*1_*active* represents the mass transferring of resist towards the outside perimeter of the column. When *path*1_*active* reaches the perimeter, either R8 or R11 will take effect and eject *mobilized_resist* into open space.

Table 6: Events of the cKMC model in Fig. 6

Number of sites involved	Reaction/transition event	Rate	Number of event
1	R1: *path*1 → *path*1_*active* (controlled)		2490
	R2: *path*2 → *mold*2 (controlled)		10470
	R3: *mold*1 → *vacancy* (controlled)		4982
	R4: *mold*2 → *vacancy* (controlled)		10470
2	R5: *path*1_*active* + *mold*1 → *mold*1 + *path*1_*active* (controlled)	1e−12	4211
	R6: *mobilized_resist* + *vacancy* → *vacancy* + *mobilized_resist* (controlled)	1.0	99259
	R7: *mobilized_resist* + *absorbent* → *vacancy* + *absorbent*	1e−12	4
	R8: *path*1_*active* + *vacancy* → *mold*1 + *mobilized_resist*	1e−12	452
	R9: *mold*1 + *resist* → *mold*1 + *mobilized_resist*	1e−2	45088
	R10: *mold*2 + *resist* → *mold*2 + *mobilized_resist*	1e−2	0
3	R11: *path*1_*active* + *vacancy* + *resist* → *mold*1 + *mobilized_resist*+ *mobilized_resist*	1e−12	2037
	R12: *mobilized_resist* + *mobilized_resist* + *resist* → *mobilized_resist* + *mobilized_resist* + *mobilized_resist*	1.0	109366
	R13: *mobilized_resist* + *vacancy* + *vacancy* → *vacancy* + *mobilized_resist* + *vacancy*	5.0	31435
	R14: *mobilized_resist* + *mobilized_resist* + *vacancy* → *mobilized_resist* + *vacancy* + *mobilized_resist*	1.0	148047
	R15: *mold*1 +*vacancy* + *resist* → *mold*1 + *mobilized_resist* + *vacancy*	1e−2	174422
	R16: *mold*2 +*vacancy* + *resist* → *mold*2 + *mobilized_resist* + *vacancy*	1e−2	0
	R17: *mobilized_resist* + *resist* + *resist* → *resist* + *resist* + *resist*	1.0	333392

R6 is a controlled event for the settling of *mobilized_resist* with the downwards direction because of gravity. R7 defines the boundary of simulation domain. R9 and R10 model the repulsive interaction between the mold and resist. R12 captures the kinetic energy transfer between *mobilized_resist*. R13 is the diffusion of *mobilized_resist*, and R14 models the coordinated diffusion between two particles. R15 and R16 model the attractive interaction between the mold and resist. Finally R17 captures the cluster formation of resist. Notice that these 17 events are by no means exhaustive. More events can be identified and included to make the model more realistic, at the

cost of simulation time.

Fig. 5-(d) and -(e) show the simulation result of two different views when the simulation stops and the mold moves upwards back to a specific position. For the selected particular set of reaction rates in the simulation, the total time used to fire a total of 976,125 events is 6308 seconds or 1.75 hours on a single-processor computer, where the rates and numbers of individual events fired are also listed in Table 6. Note that the simulation time is directly proportional to the number of events fired instead of real wall time in physical processes. The cKMC can also be parallelized and run on multi-processor computers to reduce simulation times.

Difference exists between the simulation result and the SEM image, particularly the shape of the crest. However, the difference is regarded as quantitative. Fine-tuning of rates in the existing events, such as the ones associated resist diffusion and cluster formation, the angle and directions of controlled events, the speed of mold motion, etc., can achieve better resemblance. Again, introducing more events can increase the resolution of simulation with extra computational time.

5. CONCLUDING REMARKS

In this paper, a generalized KMC mechanism, called controlled KMC, is introduced to simulate both top-down and bottom-up nanomanufacturing processes. A new concept of controlled event is introduced into the new cKMC mechanism so that events occurring at particular times, locations, or directions can be specified. Together with the traditional self-assembly events, controlled events can simulate complete physical and chemical processes. The cKMC mechanism is implemented and demonstrated by lattice-based examples of scanning probe lithography, focused beam lithography, nanoimprint lithography, and ionized physical vapor deposition.

The most important factor to accurately simulate various nanomanufacturing processes with the generic cKMC mechanism is to find simulation parameters, including a complete list of all possible events and the associated propensities or rates. This identification process usually requires full understanding the physical processes. Reaction or transition events and associated rates can be found by either physical experiments or first-principles simulation. Detailed studies with either approach are necessary for accurate KMC simulation of specific nanomanufacturing processes.

REFERENCES

[1] Lyons K.W. (2007) Integration, interoperability, and information management: What are the key issues for nanomanufacturing? *Proc. SPIE*, Vol. 6648, 66480D

[2] Xia Y., Rogers J.A., Paul K.E., and Whitesides G.M. (1999) Unconventional methods for fabricating and patterning nanostructures, *Chemical Reviews*, **99**(7): 1823-1848

[3] Busnaina A., eds. (2007) *Nanomanufacturing Handbook* (Boca Raton, FL: CRC Press)

[4] Tseng A.A., eds. (2008) *Nanofabrication: Fundamentals and Applications* (World Scientific Publishing)

[5] Komanduri R. and Raff L.M. (2001) A review on the molecular dynamics simulation of machining at the atomic scale, *Proc. Institution of Mechanical Engineer: Part B*, **215**(12), 1639-1672

[6] Fang T.-H., Weng C.-I., and Chang J.-G. (2002) Molecular dynamics simulation of nano-lithography process using atomic force microscopy. *Surface Science*, **501**: 138-147

[7] Jun S., Lee Y., Kim S.Y., and Im S. (2004) Large-scale molecular dynamics simulations of Al(111) nanoscratching. *Nanotechnology*, **15**: 1169-1174

[8] Komanduri R., Chandrasekaran N., and Raff L.M. (1998) Effect of tool geometry in nanometric cutting: a molecular dynamics simulation approach. *Wear*, **219**: 84-97

[9] Komanduri R., Chandrasekaran N., and Raff L.M. (2001) Molecular dynamics simulation of the nanometric cutting of silicon. *Philosophical Magazine B*, **81**(12): 1989-2019

[10] Yang Y., Chen S., Cheng K., and Sun X. (2007) Diamond turning of microstructured surfaces: modeling and simulation, *Int. J. of Nanomanufacturing*, **1**(5), 627-640

[11] Han X. (2007) Study micromechanism of surface planarization in the polishing technology using numerical simulation method, *Applied Surface Science*, **253**(14), 6211-6216

[12] Shimada S., Ikawa N., Inamura T., Takezawa N., Ohmori H., and Sata T. (1995) Brittle-Ductile transition phenomena in microindentation and micromachining, *CIRP Annals – Manufacturing Technology*, **44**(1), 523-526

[13] Stavropoulos P. and Chryssolouris G. (2007) Molecular dynamics simulations of laser ablation: the Morse potential function approach, *Int. J. of Nanomanufacturing*, **1**(6), 736-750

[14] Wang N., Rokhlin S.I., and Farson D.F. (2007) Nanoparticle coalescence and sintering: molecular dynamics simulation, *Int. J. of Nanomanufacturing*, **1**(6), 810-824

[15] Voter A.F. (1998) Parallel replica method for dynamics of infrequent events, *Physical Review B*, **57**(22): R13985-R13988

[16] Voter A.F. (1997) Hyperdynamics: Accelerated molecular dynamics of infrequent events, *Physical Review Letters*, **78**(20): 3908-3911

[17] Sørensen M.R. and Voter A.F. (2000) Temperature-accelerated dynamics for simulation of infrequent events, *Journal of Chemical Physics*, **112**: 9599

[18] Chatterjee A. and Vlachos D.G. (2007) An overview of spatial microscopic and accelerated kinetic Monte Carlo methods. *Journal of Computer-Aided Materials Design*, **14**:253-308

[19] Schulze T.P. (2008) Efficient kinetic Monte Carlo simulation. *Journal of Computational Physics*, **227**(4): 2455-2462

[20] Tseng A.A., Notargiacomo A., Chen T.P. (2005) Nanofabrication by scanning probe microscope lithography: A review, *Journal of Vacuum Science & Technology*, **B23**(3), 877-894

[21] Binnig G. and Rohrer H. (1985) Scanning tunneling microscopy, *Surface Science*, **152/153(**Part I**)**, 17-26

[22] Binnig G., Quate C.F., and Gerber C. (1986) Atomic force microscope, *Phys. Rev. Lett.*, **56**, 930-933

[23] Bard A.J., Fan F.R.F., Kwak J., and Lev O. (1989) Scanning electrochemical microscopy: introduction and principles, *Analytical Chemistry*, **61**(2), 132-138

[24] Liu K., Avouris Ph., Bucchignano J., Martel R., Sun S., and Michl J. (2002) Simple fabrication scheme for sub-10 nm electrode gaps using electron-beam lithography, *Applied Physics Letters*, **80**(5), 865-867

[25] Mitsuishi K., Shimojo M., Han M., and Furuya K. (2003) Electron-beam-induced deposition using a subnanometer-sized probe of high-energy electrons, *Applied Physics Letters*, **83**(10), 2064-2066

[26] van Dorp W.F., van Someren B., Hagen C.W., and Kruit P. (2005) Approaching the resolution limit of nanometer-scale electron beam-induced deposition, *Nano Letters*, **5**(7), 1303-1307

[27] Phaneuf M.W. (1999) Applications of focused ion beam microscopy to materials science specimens, *Micron*, **30**(3), 277-288

[28] Tseng A.A. (2004) Recent developments in micromilling using focused ion beam technology, *Journal of Micromechanics & Microengineering*, **14**(4), R15-R34

[29] Cabrini S., Carpentiero A., Kumar R., Businaro L., Candeloro P., Prasciolu M., Gosparini A., Andreani C., DeVittorio M., Stomeo T., and DiFabrizio E. (2005) Focused ion beam lithography for two dimensional array structures for photonic applications, *Microelectronic Engineering*, **78-79**, 11-15

[30] Young R.J., Cleaver J.R.A., and Ahmed H. (1993) Characteristics of gas-assisted focused ion beam etching, *Journal of Vacuum Science & Technology*, **B11**(2), 234-241

[31] Lee M.-K. and Kuo K.-K. (2008) Gas-assisted focused ion beam etching of indium-tin oxide film, *Japanese Journal of Applied Physics*, **47**(1), 347-350

[32] Sadki E.S., Ooi S., and Hirata K. (2004) Focused-ion-beam-induced deposition of superconducting nanowires, *Applied Physics Letters*, **85**(25), 6206-6208

[33] Xia Y. and Whitesides G.M. (1998) Soft lithography, *Annual Review of Material Science*, **28**, 153-184

[34] Rogers J.A. and Nuzzo R.G. (2005) Recent progress in soft lithography, *Materials Today*, **8**(2), 50-56

[35] Jeon S., Park J.-U., Cirelli R., Yang S., Heitzman C.E., Braun P.V., Kenis P.J.A., and Rogers J.A. (2004) *Proceedings of National Academy of Sciences*, **101**(34), 12428-12433

[36] Sotomayor Torres C.M., Zankovych S., Seekamp J., Kam A.P., Clavijo Cedeño Hoffmann T., Ahopelto J., Reuther F., Pfeiffer K., Bleidiessel G., Gruetzner G., Maximov M.V., and Heidari B. (2003), Nanoimprint lithography: an alternative nanofabrication approach, *Materials Science & Engineering C*, **23**(1-2): 23-31

[37] Guo L.J. (2004) Recent progress in nanoimprint technology and its applications, *Journal of Physics D: Applied Physics*, **37**(11): R123-R141

[38] Kumar G., Tang H.X., and Schroers J. (2009) Nanomoulding with amorphous metals, *Nature*, **457**: 868-872

[39] Choy K.L. (2003) Chemical vapour deposition of coatings, *Progress in Materials Science*, **48**, 57-170

[40] Pan Z.W., Xie S.S., Chang B.H., Sun L.F., Zhou W.Y., and Wang G. (1999) Direct growth of aligned open carbon nanotube by chemical vapor deposition, *Chemical Physics Letters*, **299**(1), 97-102

[41] Lee C.J., Kim D.W., Lee T.J., Choi Y.C., Park Y.S., Lee Y.H., Choi W.B., Lee N.S., Park G.-S., and Kim J.M. (1999) Synthesis of aligned carbon nanotubes using thermal chemical vapor deposition, *Chemical Physics Letters*, **312**(5-6), 461-468

[42] Pung, S.-Y., Choy, K.-L., Hou, X., and Shan, C. (2008) Preferential growth of ZnO thin films by the atomic layer deposition technique, *Nanotechnology*, **19**, 435609(1-8)

[43] Matsui, S., Kaito, T., Fujita, J., Komuro, M., Kanda, K., and Haruyama, Y. (2000) Three-dimensional nanostructure fabricated by focused-ion-beam chemical vapor deposition, *Journal of Vacuum Science & Technology*, **B18**(6), 3181-3184

[44] Mattox, D.M. (1998) *Handbook of Physical Vapor Deposition (PVD) Processing* (Westwood, NJ: Noyes Publications)

[45] Singh, J. and Wolfe, D.E. (2005) Review: Nano and macro-structured component fabrication by electron beam-physical vapor deposition (EB-PVD), *Journal of materials Science*, **40**(1), 1-26

[46] Salaita, K., Wang, Y., and Mirkin, C.A. (2007) Applications of dip-pen nanolithography, *Nature Nanotechnology*, **2**, 145-155

[47] Hong, S., Zhu, J., and Mirkin, C.A. (1999) Multiple ink nanolithography: towards a multiple-pen nano-plotter, *Science*, **286**(5439), 523-525

[48] Salaita, K., Wang, Y., Fragala, J., Vega, R.A., Mirkin, C.A. (2006) Massively parallel dip-pen nanolithography with 55,000-pen two-dimensional arrays, *Angew. Chem. Int. Edn*, **45**(43), 7220-7223

[49] Huo F., Zheng Z., Zheng G., Giam L.R., Zhang H., and Mirkin C.A. (2008) Polymer pen lithography. *Science*, **321**(5896): 1658-1660

[50] Lasrado, V., Alhat, D., and Wang, Y. (2008) A Review of Recent Phase Transition Simulation Methods: Transition Path Search. *Proc. 2008 ASME International Design Engineering Technical Conferences & The Computer and Information in Engineering Conference (IDETC/CIE2008)*, Paper No.DETC2008-49410

[51] Alhat, D., Lasrado, V., and Wang, Y. (2008) A Review of Recent Phase Transition Simulation Methods: Saddle Point Search. Proc. 2008 ASME International Design Engineering Technical Conferences & The Computer and Information in Engineering Conference (IDETC/CIE2008), Paper No.DETC2008-49411

[52] Gillespie D.T. (1976) A general method for numerically simulating the stochastic evolution of coupled chemical reactions. *Journal of Computational Physics*, **22**: 403-434

[53] Wang, Y. (2011) Reliable kinetic Monte Carlo simulation based on random set sampling. *Proc. 2011 ASME International Design Engineering Technical Conferences & The Computer and Information in Engineering Conference (IDETC/CIE2011)*, Paper No.DETC2011-48575

[54] Yang Y.G., Johnson R.A., and Wadley H.N.G. (1997) A Monte Carlo simulation of the physical vapor deposition of nickel, *Acta Materialia*, **45**(4): 1455-1468

[55] Huang H., Gilmer G.H., and Diaz de la Rubia T. (1998) An atomistic simulator for thin film deposition in three dimensions, *Journal of Applied Physics*, **84**(7): 3636-3649

[56] Yang Y.G., Zhou X.W., Johnson R.A., and Wadley H.N.G. (2001) Monte Carlo simulation of hyperthermal physical vapor deposition. *Acta Materialia*, **49**: 3321-3332

[57] Wang L. and Clancy P. (2001) Kinetic Monte Carlo simulation of the growth of polycrystalline Cu films. *Surface Science*, **473**: 25-38

[58] Dalla Torre J., Bilmer G.H., Windt D.L., Kalyanaraman R., Baumann F.H., O'Sullivan P.L., Sapjeta J., Diaz de la Rubia T., Djafari Rouhani M. (2003) Microstructure of thin tantalum films sputtered onto inclined substrates: Experiments and atomistic simulations. *Journal of Applied Physics*, **94**(1): 263-271

[59] Battaile C.C., Srolovitz D.J., and Butler J.E. (1997) A kinetic Monte Carlo method for the atomic-scale simulation of chemical vapor deposition: Application to diamond. *Journal of Applied Physics*, **82**(12): 6293-6300

[60] Battaile C.C. and Srolovitz D.J. (2002) Kinetic Monte Carlo simulation of chemical vapor deposition. *Annual Review of Materials Research*, **32**: 297-319

[61] Grujicic M. and Lai S.G. (1999) Atomistic simulation of chemical vapor deposition of (111)-oriented diamond film using a kinetic Monte Carlo method. *Journal of Materials Science*, **34**: 7-20

[62] Kalke M. and Baxter D.V. (2001) A kinetic Monte Carlo simulation of chemical vapor deposition: non-monotonic variation of surface roughness with growth temperature. *Surface Science*, **477**: 95-101

[63] Flidr, J., Huang, Y.-C., Newton, T.A., and Hines, M.A. (1998) Extracting site-specific reaction rates from steady state surface morphologies: Kinetic Monte Carlo simulations of aqueous Si(111) etching. *Journal of Chemical Physics*, **108**(13): 5542-5553

[64] Netto A. and Frenklach M. (2005) Kinetic Monte Carlo simulations of CVD diamond growth – interlay among growth, etching, and migration. *Diamond & Related Materials*, **14**: 1630-1646

[65] Zhou H., Fu J., and Silver R.M. (2007) Time-resolved kinematic Monte-Carlo simulation study on Si(111) etching. *Journal of Physical Chemistry*, **111**: 3566-3574

[66] Battaile C.C., Srolovitz D.J., Oleinik I.I., Pettifor D.G., Sutton A.P., Harris S.J., and Butler J.E. (1999) Etching effects during the chemical vapor deposition of (100) diamond. *Journal of Chemical Physics*, **111**(9): 4291-4299

[67] Kratzer P. and Scheffler M. (2002) Reaction-limited island nucleation in molecular beam epitaxy of compound semiconductors. *Physical Review Letters*, **88**(3): 036102(1-4)

[68] Mei D., Ge Q., Neurock M., Kieken L., and Lerou J. (2004) First-principles-based kinetic Monte Carlo simulation of nitric oxide decomposition over Pt and Rh surfaces under lean-burn conditions. *Molecular Physics*, **102**(4): 361-369

[69] Stumpf R. and Scheffler M. (1994) Theory of self-diffusion at and growth of Al(111). *Physical Review Letters*, **72**(2): 254-257

[70] Bogicevic A., Hyldgaard P., Wahnström G., and Lundqvist B.I. (1998) Al dimmer dynamics on Al(111). *Physical Review Letters*, **81**(1): 172-175

[71] Prasad M., Conforti P.F., Garrison B.J., and Yingling Y.G. (2007) Computational investigation into the mechanisms of UV ablation of poly(methyl methacrylate). *Applied Surface Science*, **253**: 6382-6385

[72] SPPARKS Kinetic Monte Carlo Simulator, available at http://www.cs.sandia.gov/~sjplimp/spparks.html

[73] Zankovych S., Hoffmann T., Seekamp J., Bruch J.-U., and Sotomayor Torres C.M. (2001) Nanoimporint lightography: challenges and prospects. *Nanotechnology*, **12**: 91-95